Supplementary Information (SI) for Journal of Materials Chemistry A.
This journal is © The Royal Society of Chemistry 2026

Supporting information

PbI_2 Interface Reconstruction Suppresses Ion Migration for Stable Planar Perovskite Solar Cells

Junxue Guo,[ab#] Zhanjun Zhu,[bc#] Yang Li,[bc] Yang Liu,[d] RuiZhi Duan,[bc] Yu Qiao,[bc] Qi Li,[bc] Bo Zhou,[bc] Wei Yu,*[bc] Can Li*[abc]

[a] *School of Chemistry and Materials Science, University of Science and Technology of China, Hefei 230026, China*

[b] *Key Laboratory of Photoelectric Conversion and Utilization of Solar Energy, State Key Laboratory of Catalysis, Dalian National Laboratory for Clean Energy, Dalian Institute of Chemical Physics, Chinese Academy of Sciences, Dalian 116023, Liaoning, China*

[c] *University of Chinese Academy of Sciences, Beijing 100049, China*

[d] *School of Materials Science and Engineering (MSE), NingboTech University, Ningbo 315211, Zhejiang, China*

[#] *These authors contributed equally.*

[*] Corresponding author

E-mail: wyu@dicp.ac.cn; canli@dicp.ac.cn

Experimental Section

Materials: Lead (II) iodide (PbI_2, ultrapure), 2,2′,7,7′-Tetrakis(N,N-dipmethoxyphenylamine)-9,9′-spirobifluorene) (Spiro-OMeTAD, 99.99%), methylammonium chloride (MACl, 99.5%), methylammonium bromide (MABr, 99.5%), Phenylethylamine iodine (PEAI) were purchased from Yuri Solar Co., Ltd. Liquid crystal molecule 4-butoxybenzylidene-4-cyanoaniline was purchased from Meryer (Shanghai) Chemical Technology Co., Ltd. Indium-doped tin oxide (ITO) glass substrates (15 Ω sq^{-1}) and formamidine iodide (FAI, 99.5%) were purchased from Advanced Election Technology Co., Ltd. The tin (IV) oxide hydrocolloid dispersion (SnO_2, 15wt%) was obtained from Alfa-Aesar. Rubidium chloride (RbCl), N, N-dimethylformamide (DMF, anhydrous), dimethyl sulfoxide (DMSO, anhydrous), isopropanol (IPA, anhydrous), chlorobenzene (CB, anhydrous), lithium bis(trifluoromethanesulfonyl) imide (Li-TFSI) and 4-t-butylphenylammonium iodide (tBP) were purchased from Sigma-Aldrich. All materials were used without any further purification.

Device fabrication: The ITO glass was cleaned in deionized water, ethanol, and isopropyl alcohol sequentially, then treated with ultraviolet ozone (UVO) for 20 min to improve its wettability. The SnO_2 precursor solution (diluted by water with the ratio of SnO_2:H_2O=1:4, v/v) was spin-coated on the ITO at 4000 rpm for 30 s and annealed at 150°C for 30 min in ambient air, then the substrates were treated by UVO for 20 min. To prepare the perovskite precursor solutions, 1.5 M PbI_2, 0.9 mg RbCl in DMF:DMSO=9:1 (v/v) was stirred for 2 h at 70°C and filtered with a 0.22 μm polytetrafluoroethylene (PTFE) filter, and the organic ammonium salt solutions (FAI: MACl=90:11 mg in 1 mL IPA) was stirred at room temperature. For BBCA-treated solution, different concentrations of BBCA (0.3, 0.5, 0.7, 1 mg) were added in organic ammonium salt solution, stirred at room temperature and filtered with a 0.22 μm PTFE filter before spin coating. 60 μL PbI_2 solution was spin-coated onto ITO/SnO_2 substrate at 1500 rpm for 30 s and then annealed at 70°C for 1 min. After the films were cooled down to room temperature, 80 μL filtered organic salt solution with and without BBCA was spin-coated on the PbI_2 film at 1800 rpm for 30 s. Then, the films were annealed

in atmosphere (30%-40% relative humidity) at 150°C for 15 min. For the PEAI treatment, 5 mg mL^{-1} PEAI in IPA was spin-coated on the perovskite film at 4000 rpm for 30 s. The hole transporting layer was fabricated on top of the perovskite film by spin-coating the spiro-OMeTAD solution at 3500 rpm for 30 s with the composition of 72.3 mg sprio-OMeTAD, 17.5 μL Li-TFSI solution (520 mg in 1 mL acetonitrile), 28.8 μL tBP solution in 1 mL chlorobenzene. Finally, 100 nm Au was deposited via thermal evaporation at 4×10^{-4} Pa.

Characterizations and measurements: The current-voltage (*J-V*) measurement and steady-state power output of the devices were performed on Keithley 2400 Series Source Meter under standard AM 1.5G illumination via a solar simulator (SS-F5-3A, Enlitech), and the light intensity was calibrated to 100 mW cm^{-2} using a calibrated silicon reference cell. The devices were measured both in reverse scan (1.2 V~ –0.1 V, step 0.02 V) and forward scan (–0.1 V~1.2 V, step 0.02 V), and the delay time was 20 ms. The devices were measured without an aperture mask during *J-V* testing. The external quantum efficiency (EQE) data were obtained by using the solar-cell spectral-response measurement system (QE-R, Enlitech), which was calibrated by a certified silicon solar cell. A small, consistent discrepancy (~5-7%) was observed between the J_{SC} values obtained from *J-V* curves and those integrated from EQE spectra. This is primarily attributed to the lack of an aperture mask during *J-V* measurement, which can lead to a slight overestimation due to scattered light, a phenomenon commonly reported in the literature. All conclusions regarding the comparative performance between device groups are unaffected, as identical measurement conditions were applied.

Thermogravimetric (TG) analysis was obtained by Diamond TG/DTA, with a heating rate of 10℃ min^{-1}, and a carrier gas flow rate of 20 mL min^{-1}. Differential scanning calorimetry (DSC) was obtained by TA Q20 to determine the melting point and phase transition temperatures of BBCA molecule. Polarizing microscope (POM) was carried out on OLYMPUS GX71 to analyze the optical properties of crystals.

The scanning electron microscope (SEM) images were obtained by a field emission scanning electron microscopy (JSM-7900F, Japan), where the electron beam was accelerated at 3 kV. The X-ray diffraction (XRD) patterns were attained by Rigaku

SmartLab with Cu Kα radiation (200 mA and 40 kV) in a step of 0.01°. The incident angle from 5° to 60°, and the scanning speed was 10° min^{-1}. The time-of-flight secondary-ion mass spectrometry (ToF-SIMS) measurement was performed on the ToF SIMS M6 (ION-TOF GmbH, Germany). The UV-Vis absorption spectra were measured by Cary 5000 UV-Vis-NIR spectrophotometer, Varian Inc, USA. The steady-state PL spectra and time-resolved PL spectra were recorded on a FLS920 fluorescence spectrometer (Edinburgh Instruments) in air at room temperature. A picosecond pulsed diode laser (406.8 nm) was used as the excitation source. Grazing-incidence wide-angle X-ray scattering (GIWAXS) was tested using the Shanghai Synchrotron Radiation Facility (SSRF) Beamline BL14B1 with the incident photon energy of 10 keV (wavelength of 1.2398 Å) at an incident angle of 0.4° and an exposure time of 30 s. The samples for GIWAXS measurement were prepared on Glass/ITO substrates as the same condition used for devices. The ^{1}H NMR measurement in solution was carried out on the Bruker AVANCE III 400 (400 MHz) spectrometer at room temperature, with TMS as internal standard reference. The X-ray photoelectron spectroscopy (XPS) was carried out on an ESCALAB 250Xi photoelectron spectroscopy (Thermo Fisher Scientific) with Al Kα radiation source and all the binding energies were calibrated by C 1s (284.8 eV) as a reference. The UPS measurements were carried out with VG Scientia R3000 analyzer in ultrahigh vacuum with a base pressure of 1×10^{-10} mbar. The HOMO energy level (E_{HOMO}) was calculated by the equation $E_{HOMO}=-[21.22-(E_{cutoff}-E_{F,\ edge})]$, where the E_{cutoff} and the $E_{F,\ edge}$ represent the cut-off energy region and the Fermi edge region in the UPS spectra, respectively.

The hole trap densities of devices with or without BBCA treated were measured by space-charge-limited-current (SCLC) method with hole-only devices: ITO/PEDOT:PSS/perovskite/spiro-OMeTAD/Au, respectively, in dark at –0.1~5 V by Keithley 2400 Series Source Meter. Mott-Schottky analysis was conducted on IVIUMSTAT electrochemical workstation at 10 kHz, with a 20 mV AC amplitude and a voltage range of 0~1.5 V. Electrochemical impedance spectroscopy (EIS) was conducted in the dark at room temperature using a Gamry electrochemical workstation,

with a 0.98 V bias and frequency range from 260 kHz to 5 Hz.

Computational calculation: The Gaussian 09 program package of m062x/def2svp is used for calculations of the most stable molecular configurations and the m062x/def2tzvp is for binding energies calculations of BBCA, FAI and PbI_2 molecules. The calculation of BBCA on perovskite surface is performed using the VASP code [1-2] based on the density functional theory. For the exchange-correlation functional, the generalized gradient approximation (GGA) of Perdew-Burke-Ernzerhof (PBE) is used [3]. The projector augmented-wave pseudopotentials are used with an energy cutoff of 500 eV for the plane-wave basis functions. In all calculations, van der Waals (vdW) interactions were accounted for at the D3 level [4]. For all of the calculations, the vacuum regions between the slabs were more than 20 Å. The Brillouin zone integration is carried out using 3×3×1 Monkhorst−Pack k-point meshes. The structures were relaxed until the force on each atom was smaller than 0.02 eV/Å. The convergence criterion for the electronic self-consistency was 10^{-6} eV. The symmetry was switched off during structural relaxation. For this case, the adsorption energies (E_{ads}) of adsorbates can be calculated using the following equation:

$$E_{ads} = E_{(adsorbate/surface)} - E_{(surface)} - E_{(adsorbate)}$$

where $E_{(adsorbate/surface)}$ is the total energy of the interacting system, $E_{(adsorbate)}$ and $E_{(surface)}$ are the energies of the gas-phase molecule and surface slab, respectively.

Equation S1: The dependence of V_{OC} on light intensity (P) can be presented as following:

$$Voc(P) = \frac{n\mathrm{K_B T}}{\mathrm{q}} \mathrm{In}(P) + \mathrm{C}$$

where the K_B, T, q, n and C are the Boltzmann constant, the temperature in Kelvin, the elementary charge, the ideal factor related to the dominant recombination mechanism in devices and the constant, respectively.

Equation S2. The trap density (n_t) from SCLC measurements can be calculated according to the following equation:

$$n_t = (2V_{TFL}\varepsilon_0\varepsilon)/(qL^2)$$

where ε refers to the dielectric constants of perovskite (46.9), ε_0 is the vacuum permittivity (8.85×10^{12} F m^{-1}), q is the elementary charge, and L is the thickness of perovskite films.

Equation S3. The bi-exponential equation was used to fit the TRPL decay curves as follows:

$$I(t) = I_0 + A_1 \exp(-t / \tau_1) + A_2 \exp(-t / \tau_2)$$

where A_1 and A_2 represent the decay amplitude, and τ_1, τ_2 stands for the fast and slow decay time constants, which could be ascribed to nonradiative recombination and radiative recombination, respectively.

Equation S4. The average lifetime (τ_{ave}) obtained from the TRPL decay curves is calculated by the following equation:

$$\tau_{ave} = \frac{A_1\tau_1^2 + A_2\tau_2^2}{A_1\tau_1 + A_2\tau_2}$$

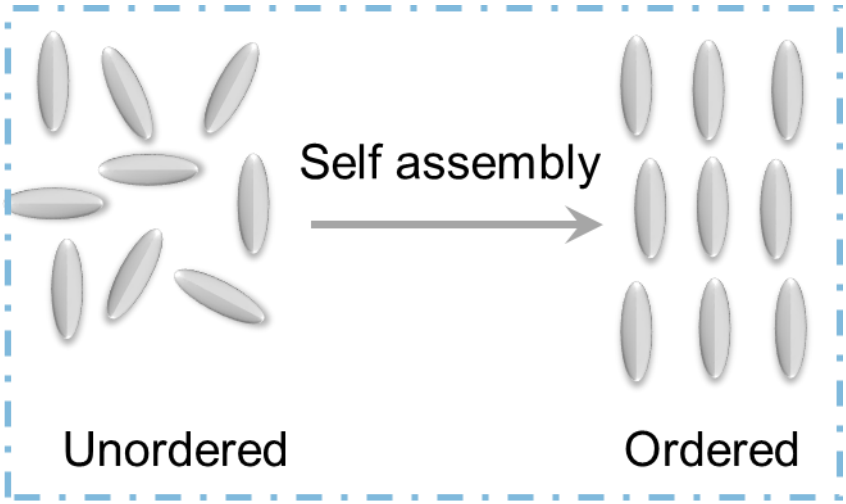

Fig. S1. The Schematic diagram of self-assembly stack after annealing of BBCA.

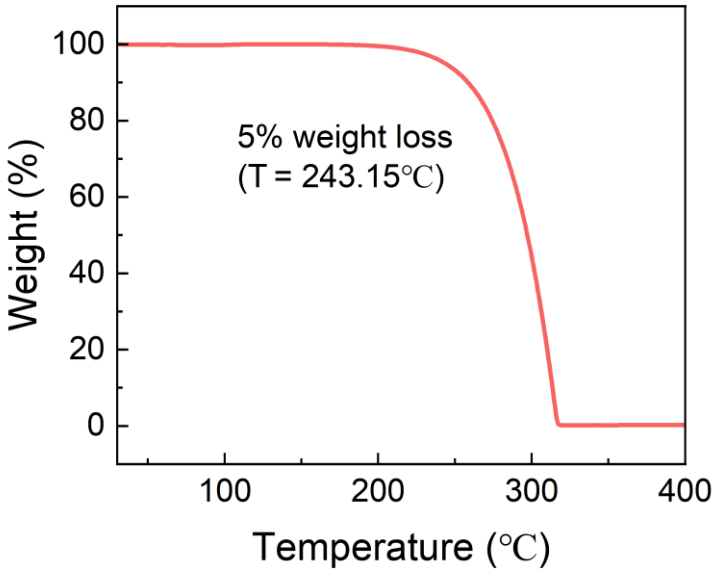

Fig. S2. The TG curve of BBCA.

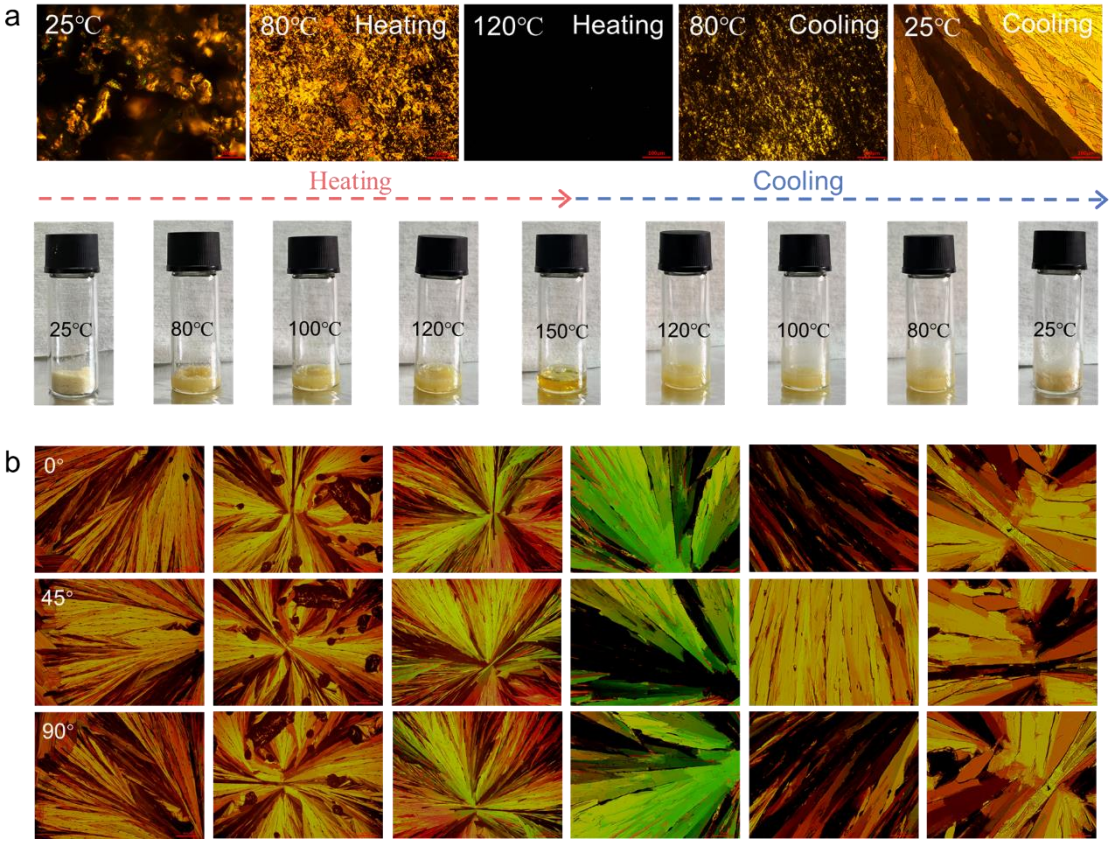

Fig. S3. (a) POM images and physical state photographs of BBCA at different temperatures during heating and cooling. (b) Full POM rotation series of BBCA liquid crystal phase at 0°, 45°, and 90° for all recorded fields of view.

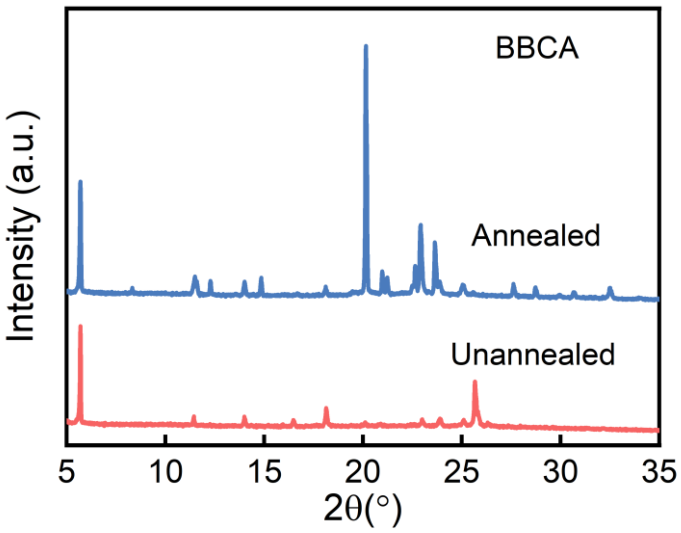

Fig. S4. XRD patterns of BBCA before and after annealing.

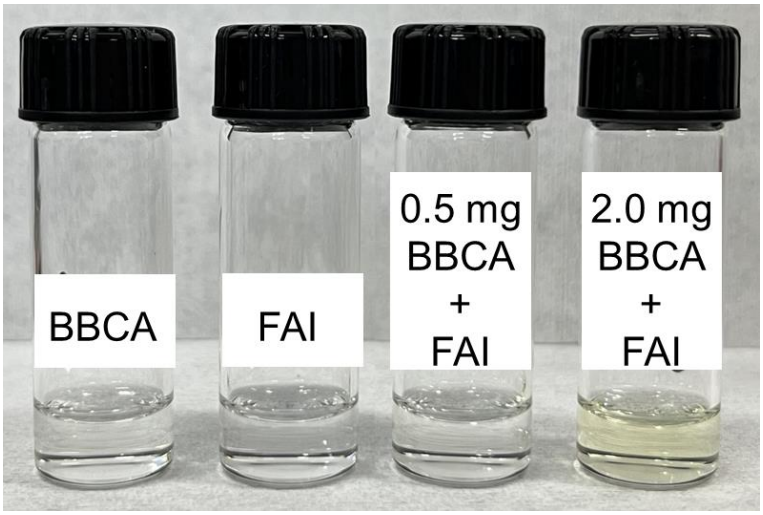

Fig. S5. Colors of BBCA, FAI, and FAI solutions containing different concentrations of BBCA.

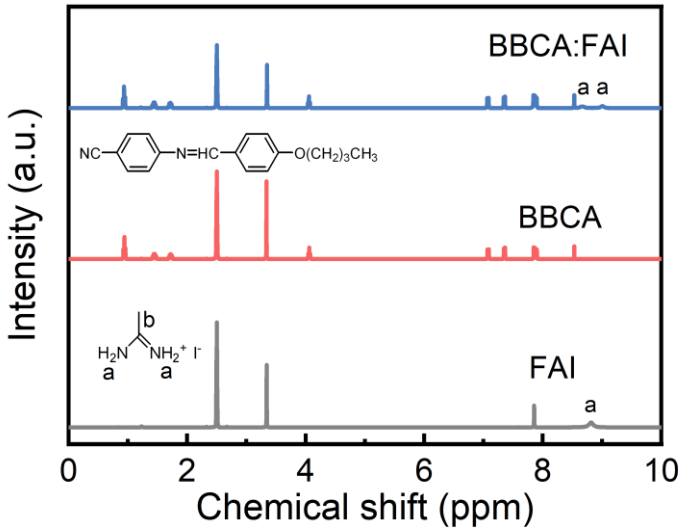

Fig. S6: ^{1}H-NMR spectra in deuterated DMSO of FAI, BBCA and BBCA:FAI mixture.

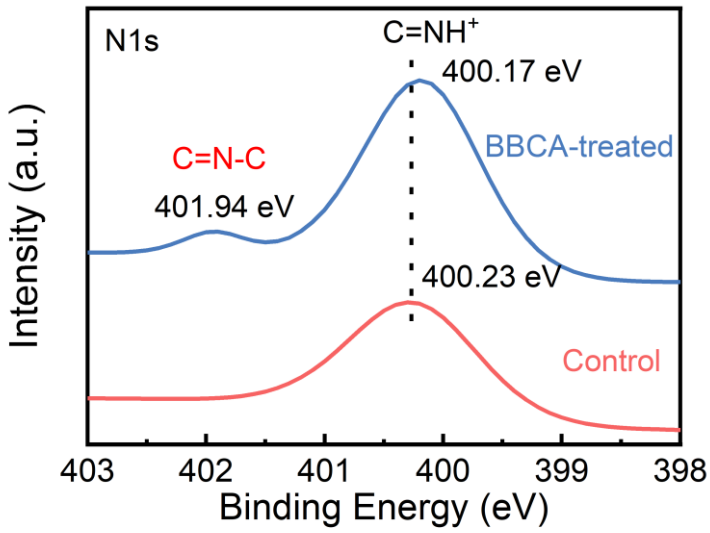

Fig. S7. N1s XPS spectra of the control and BBCA-treated films.

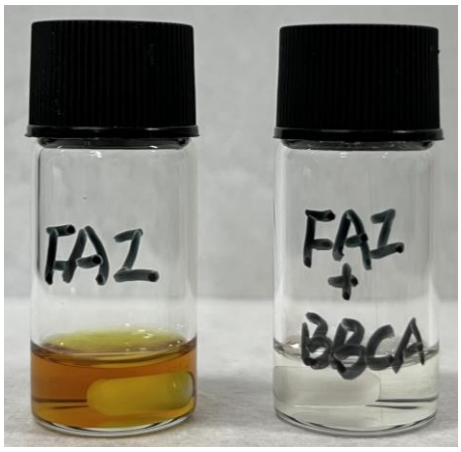

Fig. S8. The color changes of FAI and BBCA:FAI solutions after light aging.

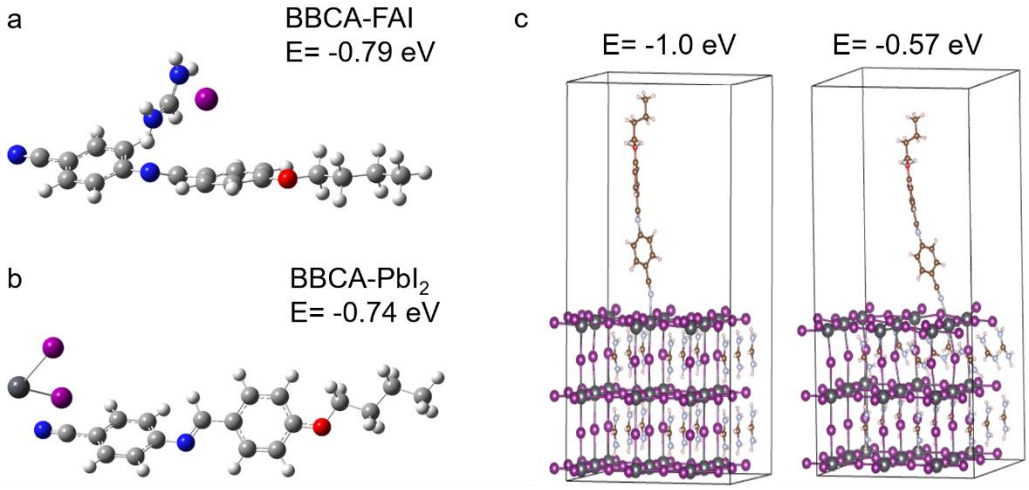

Fig. S9. Computational study of most favorable molecular configurations and binging energies of BBCA-FAI (a), BBCA-PbI_2 (b) and BBCA-$FAPbI_3$ surface (c).

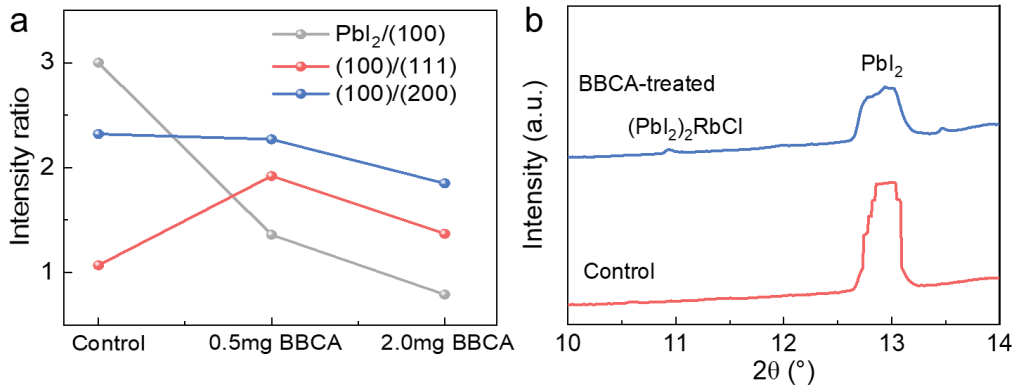

Fig. S10. (a)The peak intensity ratios of $I_{PbI2}/I_{(100)}$, $I_{(100)}/I_{(111)}$, $I_{(100)}/I_{(200)}$ planes in Fig. 2a. **(b)** The direct intensity comparison of PbI_2 extracted from GIWAXS in Fig. 2c and 2d.

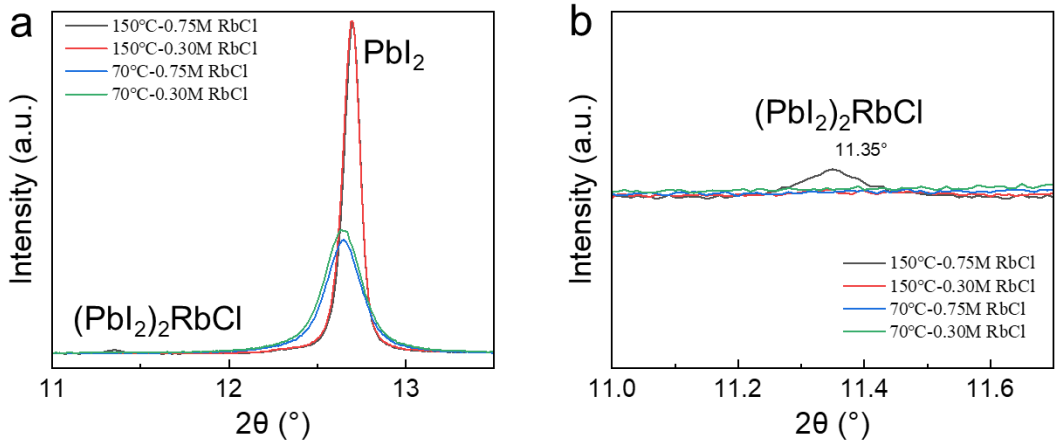

Fig. S11. XRD patterns of 1.5M PbI_2 mixed with 0.30M/0.75M RbCl films annealed at different temperatures: (a) 2θ at 11-13.5 °; (b) 2θ at 11-11.7 °.

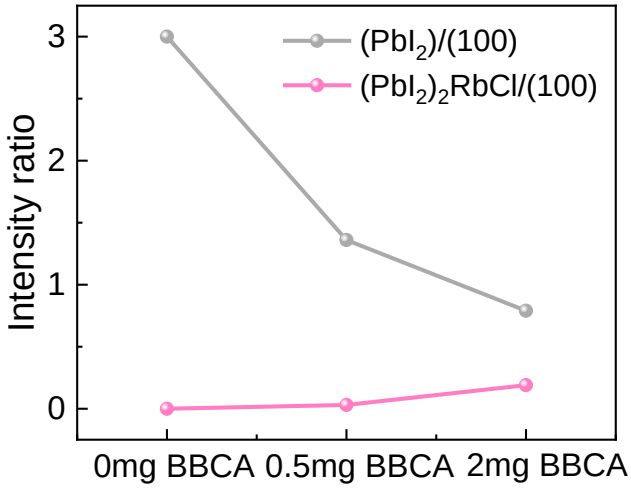

Fig. S12. The peak intensity ratios of $I_{PbI2}/I_{(100)}$ and $I_{(PbI2)2RbCl}/I(100)$ in Fig. 2a.

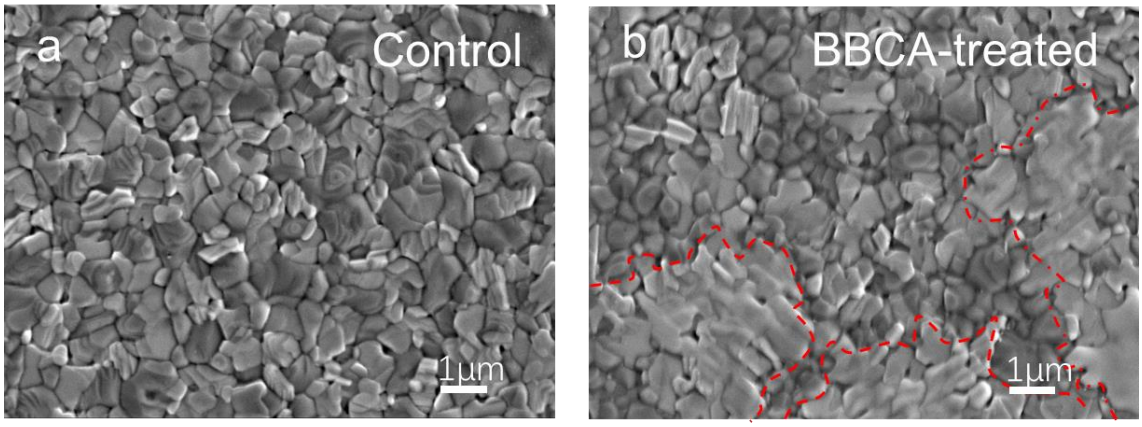

Fig. S13. Secondary electron SEM images of (a) control and (b) BBCA-treated perovskite films.

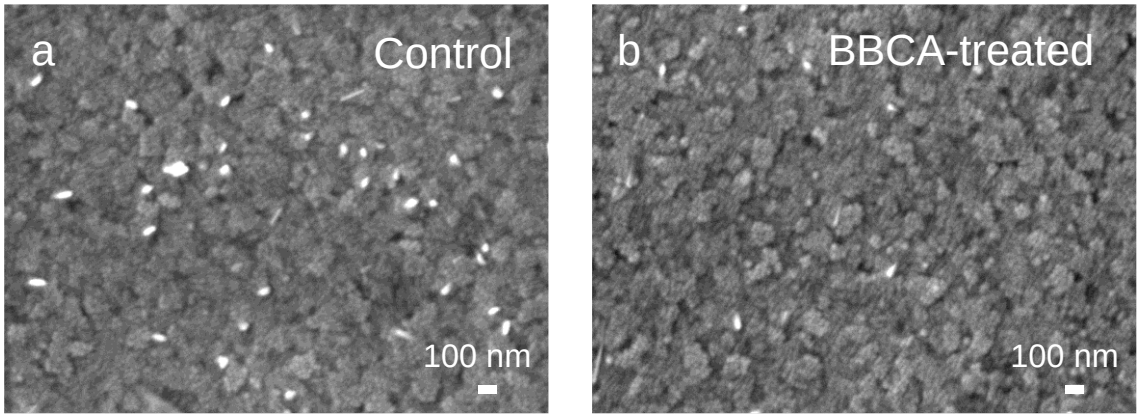

Fig. S14. SEM backscattering image of ITO after exfoliated.

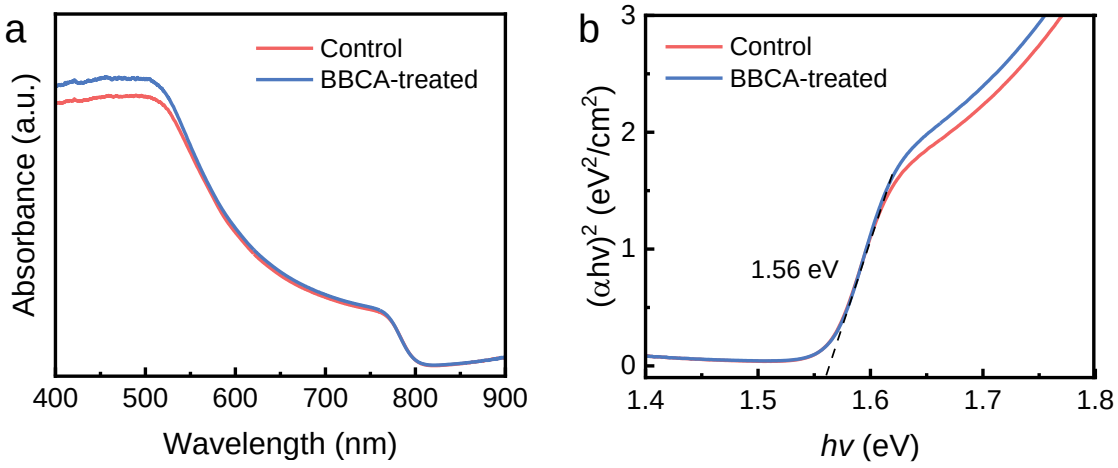

Fig. S15. (a) UV-Vis absorption spectra and (b) Tauc curves of control and BBCA-treated perovskite films.

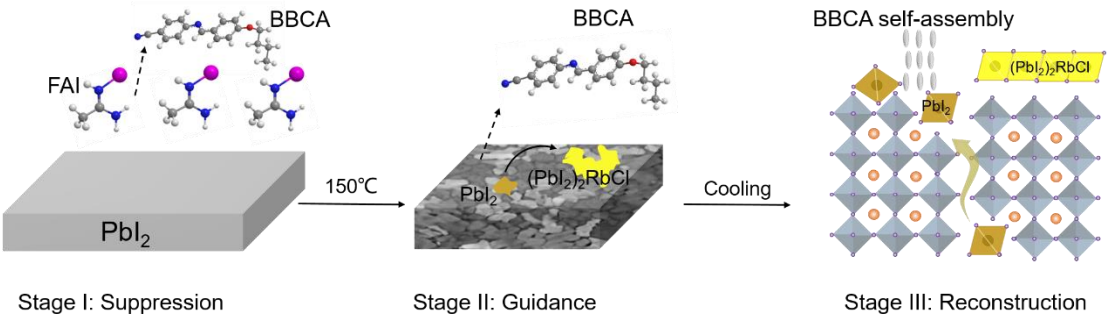

Fig. S16. Schematic diagram of the BBCA induced reconstruction PbI_2.

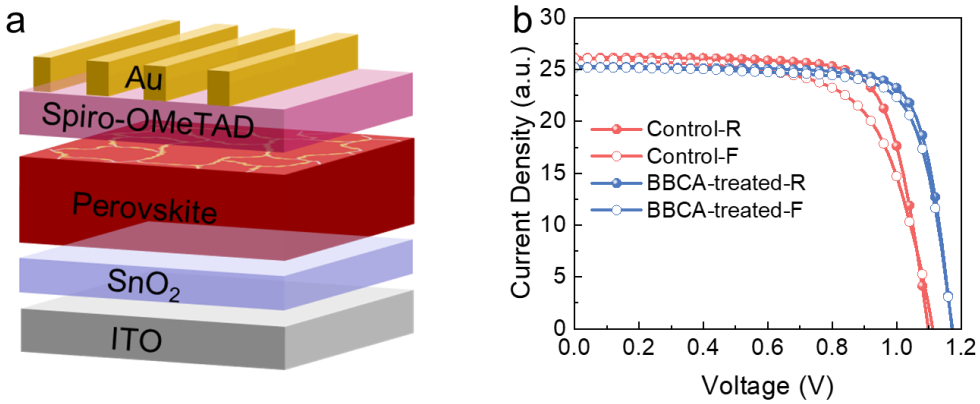

Fig. S17. (a) The device structure of perovskite solar cells; (b) Forward and reverse scan of characterization of the control and BBCA-treated devices.

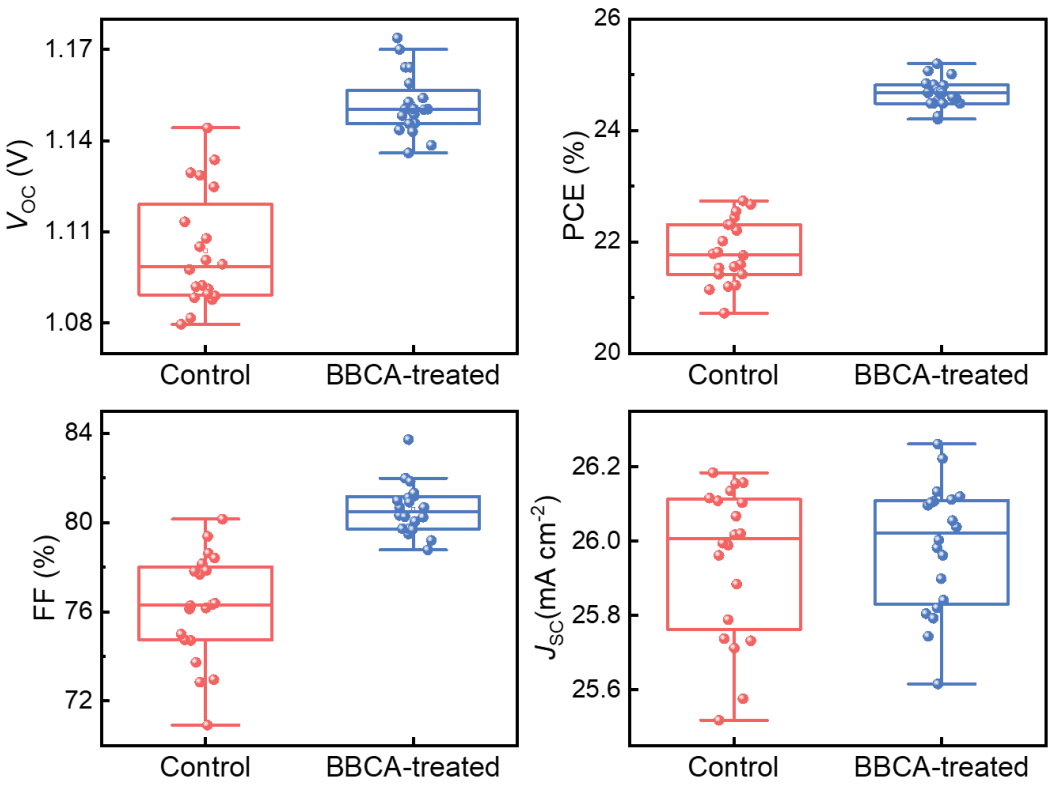

Fig. S18. The statistic distribution of photovoltaic parameters of control and BBCA treated PSCs based on 20 devices.

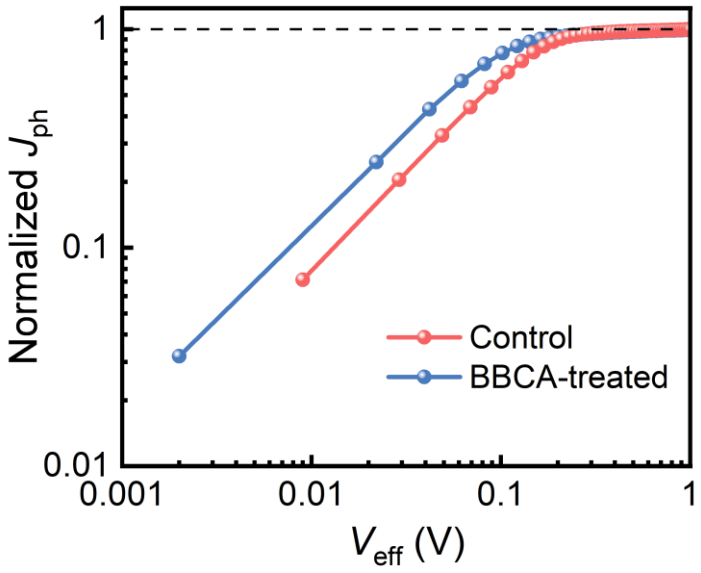

Fig. S19. Typical photocurrent density versus effective voltage curves of the control and BBCA-treated devices.

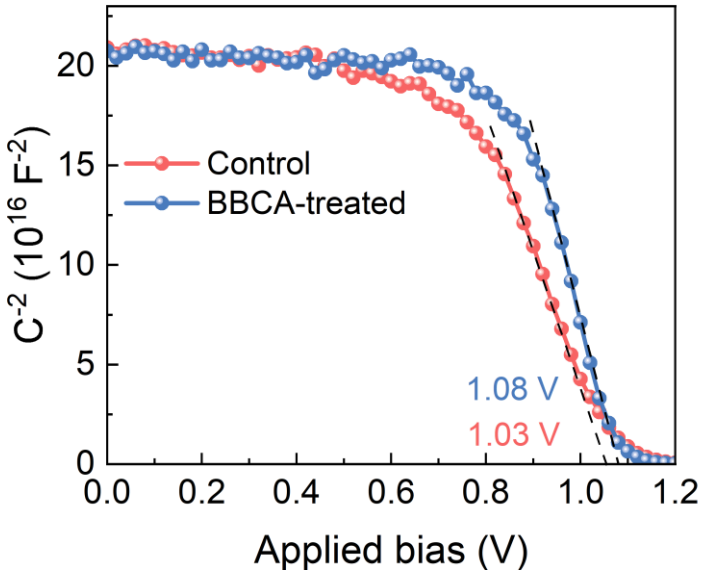

Fig. S20. Mott-Schottky plots of the control and BBCA-treated devices.

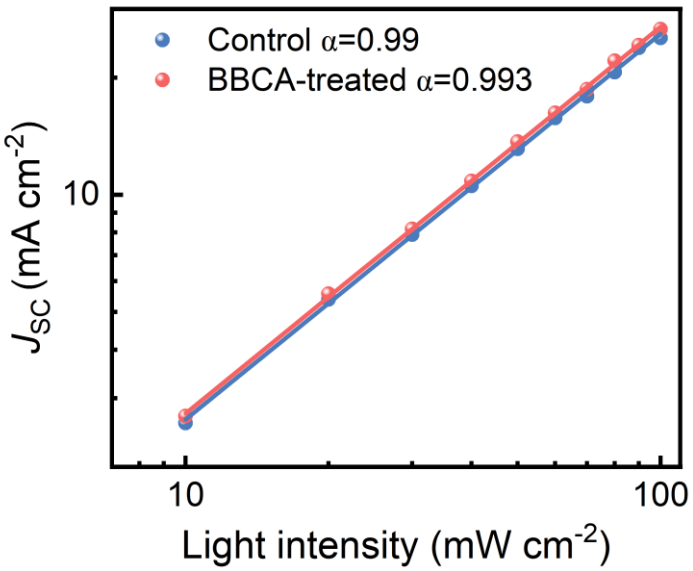

Fig. S21. The dependence of J_{SC} on light intensity for control and BBCA-treated devices.

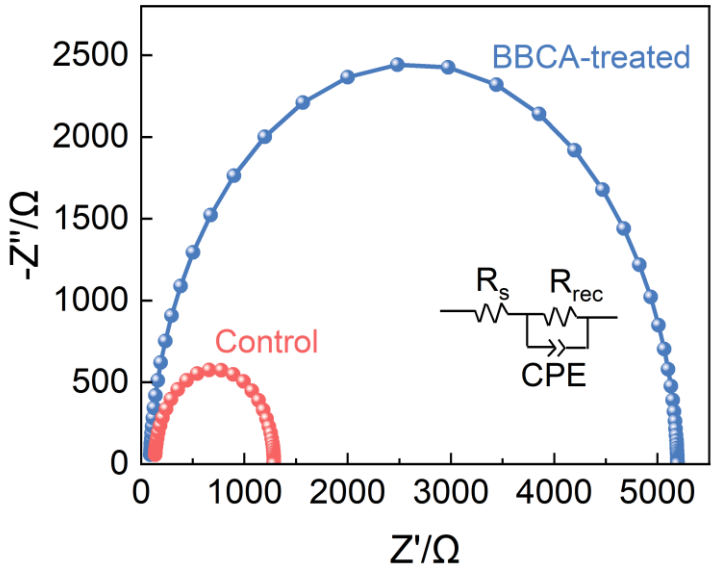

Fig. S22. Nyquist plots of the control and BBCA-treated devices.

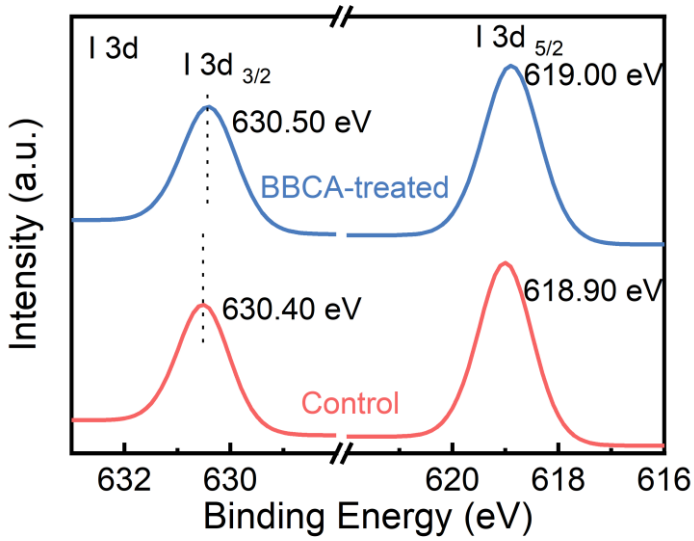

Fig. S23. I 3d XPS of control and BBCA-treated perovskite films.

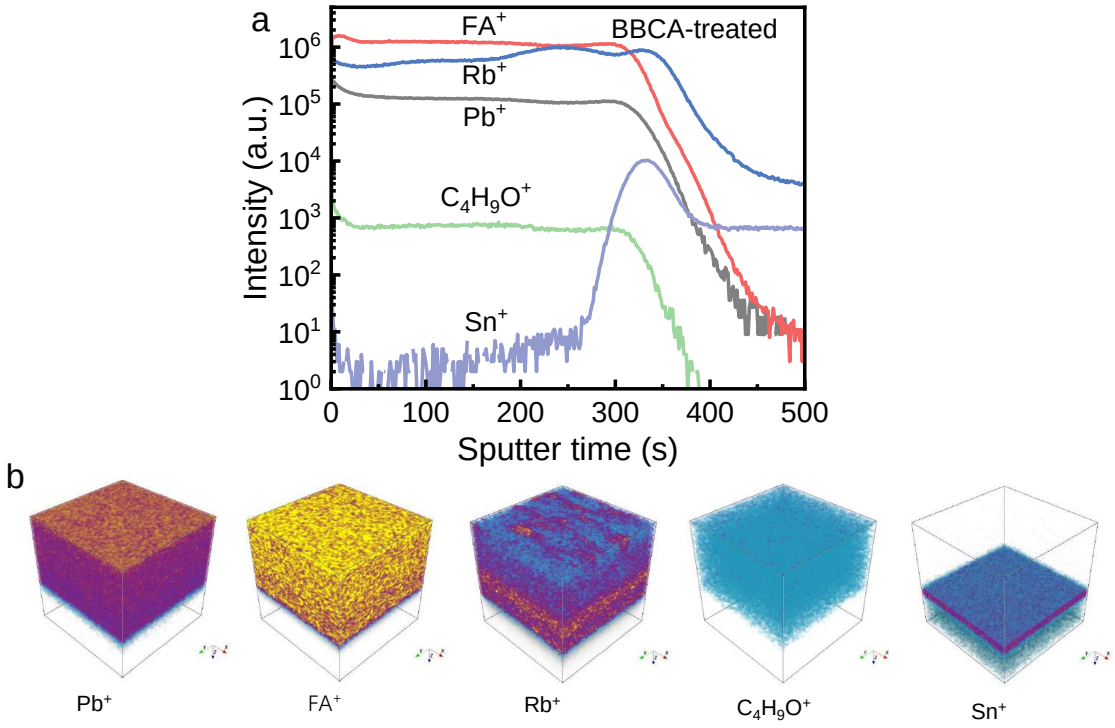

Fig. S24. (a)The ToF-SIMS depth profiles and (b) 3D mapping of Pb^+、FA^+、Rb^+、$C_4H_9O^+$ and Sn^+ in BBCA-treated perovskite film.

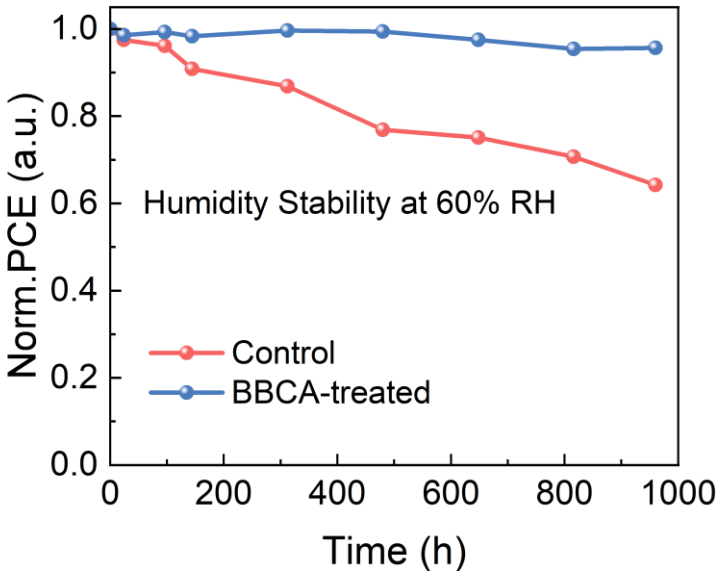

Fig. S25. Humidity stability of control and BBCA-treated PSCs without encapsulated.

Table S1. The XRD peak intensity of perovskite films and the peak intensity ratios of $I(PbI_2)/I(100)$, $I(100)/I(111)$ and $I(100)/I(200)$ planes

Name	I (PbI_2) (a.u.)	I (PbI_2)$_2$ RbCl (a.u.)	I (100) (a.u.)	I (111) (a.u.)	I (200) (a.u.)	$I(PbI_2)/I(100)$	$I(100)/I(111)$	$I(100)/I(200)$
Control	6544	0	2184	2042	939	3.00	1.07	2.32
0.5mg BBCA-treated	3700	73	2723	1421	1201	1.36	1.92	2.27
2mg BBCA-treated	1740	417	2199	1638	1189	0.79	1.37	1.85

Table S2. The XRD peak intensity of perovskite films and the peak intensity ratios of $I(PbI_2)/I(100)$.

Name		I (PbI_2) (a.u.)	I (100) (a.u.)	$I(PbI_2)/I(100)$
Control	Fresh	4643	1920	2.42
	Light-aged	10924	1510	7.23
	Thermal-aged	5203	1637	3.17
BBCA-treated	Fresh	1984	3721	0.54
	Light-aged	1839	3721	0.49
	Thermal-aged	2249	3546	0.63

Table S3. Performance parameters of PSCs with different concentrations BBCA-treated.

Name	V_{OC} (V)	J_{SC} (mA cm^{-2})	FF (%)	PCE (%)
Control	1.12	26.19	77.89	22.85
0.3mg BBCA-treated	1.14	26.00	80.24	23.78
0.5mg BBCA-treated	1.15	26.11	83.73	25.14
0.7mg BBCA-treated	1.14	26.25	79.87	23.90
1.0mg BBCA-treated	1.14	26.36	78.79	23.67

Table S4. Performance parameters of PSCs with forward and reverse scan.

Name	Scan direction	V_{OC} (V)	J_{SC} (mA cm^{-2})	FF (%)	PCE (%)	HI[a]
Control	Reverse scan	1.10	26.14	74.97	21.53	0.12
	Forward scan	1.11	26.05	65.54	18.99	
BBCA-treated	Reverse scan	1.17	25.73	76.66	23.06	0.04
	Forward scan	1.16	25.69	74.04	22.05	

[a] $\mathrm{HI} = \frac{\mathrm{PCE_{reverse}} - \mathrm{PCE_{forward}}}{\mathrm{PCE_{reverse}}}$

Table S5. The η_{cc} probability of PSCs obtained from J_{ph}-V_{eff} characteristics.

Name	0.1 V	0.2 V	1.2 V
Control	63.65%	87.64%	99.45%
BBCA-treated	77.81%	92.83%	99.78%

Table S6. Fitted parameters of EIS for the control and BBCA-treated PSCs.

Name	$R_s(\Omega)$[a)]	$R_{rec}(\Omega)$[b)]
Control	133.4	1152
BBCA-treated	81.94	5108

[a)] R_s is the series resistance of devices.

[b)] R_{rec} is the recombination resistance of devices.

Table S7. The fitting parameters of the TRPL spectra for the control and BBCA-treated perovskite films.

Name	τ_1 (ns)	A_1 (%)	τ_2 (ns)	A_2 (%)	τ_{ave} (ns)
Control	191.35	23.58	833.68	76.42	791.20
BBCA-treated	128.65	4.46	1467.47	95.54	1462.01

References

[1] G. Kresse, J. Furthmu¨ller, Efficient iterative schemes for ab initio total-energy calculations using a plane-wave basis set. Phys. Rev. B 1996, 54: 11169-11186.

[2] G. Kresse, J. Furthmiiller, Efficiency of ab-initio total energy calculations for metals and semiconductors using a plane-wave basis set. Computational Materials Science 1996, 6: 15-50.

[3] John P. Perdew, Kieron Burke, Matthias Ernzerhof, Generalized Gradient Approximation Made Simple. Phys. Rev. Lett. 1996, 77 (18): 3865-3868.

[4] S. Grimme, J. Antony, S. Ehrlich, et al., A consistent and accurate ab initio parametrization of density functional dispersion correction (DFT-D) for the 94 elements H-Pu. J Chem Phys 2010, 132 (15): 154104.